

Shielding Effectiveness Measurement for Extremely Small Dimension Enclosures

Ali Shourvarzi and Mojtaba Joodaki , Senior Member, IEEE

Abstract—In this paper, practical aspects of a newly proposed method based on the aperture impedance measurement for estimation of the shielding effectiveness (SE) of enclosures is discussed in more details. A special de-embedding procedure for this measurement is explained and practically implemented. Then, in order to show the capability of the method, we applied it to a remarkably small dimension enclosure (40 mm × 40 mm × 20 mm) with a rectangular aperture as well as to an enclosure with a triangular shape aperture. These case studies confirm the practicality of the new method for enclosures with extremely small dimension and those with arbitrary shape apertures.

Index Terms—Electromagnetic compatibility, electromagnetic shielding, scattering parameters.

I. INTRODUCTION

THE concept of electromagnetic shielding is a premier method to prevent the detrimental effects of a noise source on a disposed victim. Passing through time, the printed circuit boards (PCBs) are becoming more dense and smaller. Therefore, the shielded enclosures containing the PCBs are becoming smaller. So, the estimation of the shielding performance for small dimension enclosures is noteworthy and attractive.

The most noticeable figure of merit to judge the shield quality is shielding effectiveness (SE) [1]

$$SE_E = 20 \log(E_{\text{abs}}/E_{\text{prs}}). \quad (1)$$

In the definition above, E_{abs} and E_{prs} are the electric fields in the monitor point (a point in the shielded media) in the absence and presence of the shield, respectively.

Measuring SE for physically small dimension enclosures is a troublesome procedure. The latest standard for measuring SE of small enclosures is IEEE Std. 299.1-2013 [2], which is applicable to enclosures with dimensions as small as 12 cm. This standard requires transverse electromagnetic (TEM) cells, reverberation chambers, and accurate sensors that must be positioned precisely [2].

In 1994, an optically coupled electric field sensor was used to measure SE for small enclosures [3]. This sensor had dimension

Manuscript received July 6, 2018; revised August 20, 2018 and October 7, 2018; accepted November 9, 2018. This work was supported by Ferdowsi University of Mashhad under the Project 33482. (Corresponding author: Mojtaba Joodaki.)

The authors are with the Electrical Engineering Department, Ferdowsi University of Mashhad, Mashhad 9175656851, Iran (e-mail: ali.shourvarzi@mail.um.ac.ir; joodaki@um.ac.ir).

Color versions of one or more of the figures in this paper are available online at <http://ieeexplore.ieee.org>.

Digital Object Identifier 10.1109/TEMC.2018.2882893

of 71 mm. The frequency range was up to 2 GHz and the results were not compared to any other methods. Also, a multipoint field measurement setup was proposed using a reverberation chamber [4]. The dimensions of the device under test (DUT) in this research were 80 cm × 70 cm × 100 cm. In another work, a 10 cm × 20 cm × 30 cm enclosure was used as the DUT [5]. A dimensional scaling method was used to estimate SE for physically small and electrically large enclosures. Kubik and Skala used a finite element method to estimate SE for a 291 mm × 277 mm × 243 mm enclosure [6].

In a recently published article, the SE of an enclosure was measured using a microstrip line (MSL) placed over the aperture of the enclosure [7]. In comparison with the conventional methods, this method is accurate, low cost, less complicated, and more user friendly. Other publications of Shourvarzi and Joodaki toward introducing and enhancing the proposed method and its advantages are [8]–[12]. In [8], this approach is extended to be capable of measuring SE in more practical cases. In that article, different monitor points (the points at which the electric field is measured) are chosen. Polarization and incident angles are also arbitrary. In [9], the proposed method is used to optimize the shield structure to have the best possible SE. In this paper, this technique is improved and its applicability for extremely small dimension enclosures is demonstrated.

In Section II, a brief review of the proposed method is presented and it is enhanced to be more practical than our previous works. Section III is dedicated to a major practical point, de-embedding. In Section IV, simulation results are presented. Section V proposes the experimental setup for an extremely small dimension enclosure and compares the experimental and simulation results. The conclusions are drawn in Section VI.

II. PRINCIPLE OF OPERATION

A MSL over the aperture of the enclosure, along with two SMA ports, form a two-port network as shown in Fig. 1. Z_1 and Z_2 are the impedances of the ports and Z is the impedance seen between the ports. If the ports are ideal (50Ω), then $Z_1 = Z_2 = 50 \Omega$ (equal to the characteristic impedance of the MSL, Z_0). For a 50Ω line, $Z = 0$. But if any distortion (like an aperture) is applied to this ideal MSL, then Z will be a nonzero complex number and its value can be derived from the S -parameters as follows [14]:

$$S_{21} = \frac{V_2 - I_2 Z_0}{V_1 + I_1 Z_0} \quad (2)$$

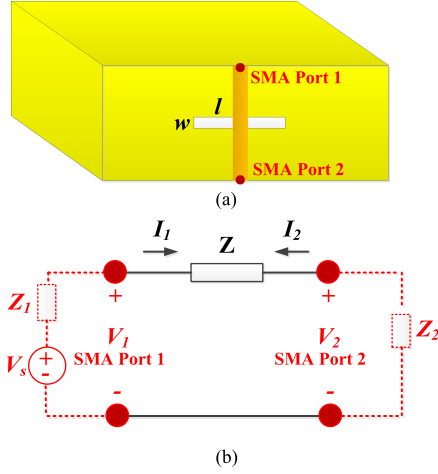


Fig. 1. (a) Enclosure with an aperture, the orange strip is the signal trace of an MSL and the enclosure is its ground plane. (b) Two port network that is an equivalent circuit for the setup in (a).

$$V_1 = V_S \frac{Z_0 + Z}{2Z_0 + Z} \quad (3)$$

$$V_2 = V_S \frac{Z_0}{2Z_0 + Z} \quad (4)$$

$$I_1 = \frac{V_S}{2Z_0 + Z} = -I_2 \quad (5)$$

$$S_{21} = \frac{2Z_0}{2Z_0 + Z} \quad (6)$$

$$Z = \frac{2Z_0(1 - S_{21})}{S_{21}}. \quad (7)$$

Z can be defined using Fig. 2. It is the parallel combination of the aperture impedance (Z_{ap}) and the transferred short circuit of the enclosure end (Z'_{SC})

$$Z_{ap} = \frac{ZZ'_{SC}}{Z'_{SC} - Z}. \quad (8)$$

Z'_{SC} is as follows:

$$Z'_{SC} = jZ_g \tan(k_g a). \quad (9)$$

In the above-mentioned equations, Z_0 is equal to 50Ω if the ports are ideal. If we consider the enclosure as a waveguide, k_g and Z_g are its propagation constant and the characteristic impedance, respectively. S_{21} is the result of the simple S -parameter analysis in Fig. 1. It should be noted that any losses in the enclosure are incorporated into the aperture impedance.

Now, we can estimate SE of the enclosure by using the derived aperture impedance and the equivalent circuit presented in Fig. 2. In order to calculate SE, based on (1), the amount of the leaked electric field into the enclosure is needed. By assuming the incident wave as a voltage source (v_s) and the free space impedance ($\eta_0 = 377 \Omega$) as the source impedance, then the aperture impedance as the load at point A is obtained. Using the network theory, one can measure the amount of the leaked voltage at the monitor point [P (p_x, p_y, p_z)] and finally the SE

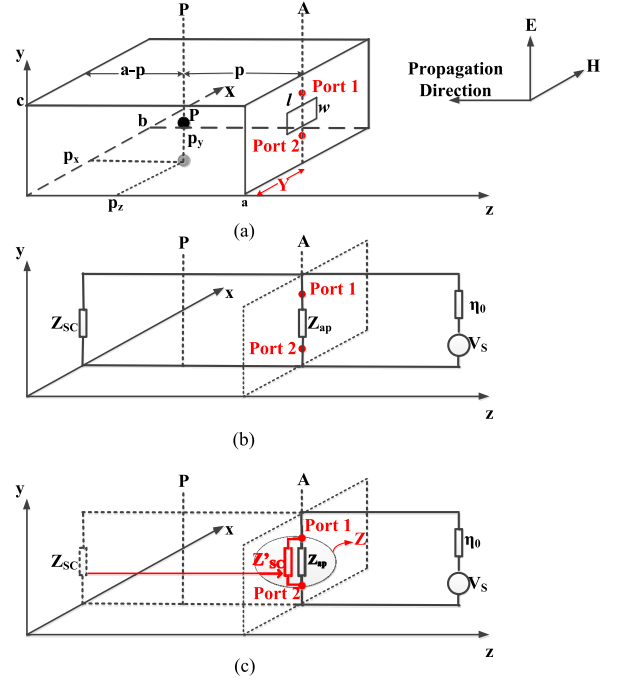


Fig. 2. (a) Enclosure with aperture and the incident plane wave. (b) Circuit model for the enclosure with aperture. (c) Circuit model for the enclosure with transferred impedance of the end short circuit [7].

can be evaluated [7]. Since SE is based on Z_{ap} and Z_{ap} in turn is derived in terms of S_{21} [using (2)–(8)], SE can be expressed in terms of S_{21} . SE can also be expressed as a function of S_{11} as presented in [7].

As the Z_{ap} is the basic parameter that is used to determine SE, two important questions must be addressed here. The first one is whether the Z_{ap} influence on SE is accurately measurable in real applications or it is masked by a parallel low value Z'_{SC} . The second question is the accuracy of our measured Z_{ap} in practice. In order to answer the first question, the SE sensitivity to Z_{ap} must be calculated. Relying on the Thevenin's theory and Robinson's equations, the relation between SE and Z_{ap} is obvious [13] and the SE sensitivity to Z_{ap} at the frequency of f_0 , can be calculated as

$$S(f_0) = \frac{\partial(\text{SE})}{\partial(Z_{ap})} \Big|_{f=f_0} \times 100\%. \quad (10)$$

Fig. 3 shows the calculated S versus frequency for an enclosure with an aperture in the center of its front face. The results present considerable changes in SE due to Z_{ap} variations even at higher frequencies.

Regarding the second point, the real and imaginary parts of our extracted Z are compared with those of computed Z using three-dimensional full-wave simulator of CST-MWS (CST Studio Suite 2017). The solver properties are as follows: frequency domain solver, tetrahedral (legacy) mesh type, accuracy of 10^{-9} and mesh cells number of 74 412. As shown in Fig. 4, the results are in excellent agreement with each other. The maximum difference (that occurs at 1 GHz) is less than 2Ω that is equal to 4.5% of the desired impedance at that frequency.

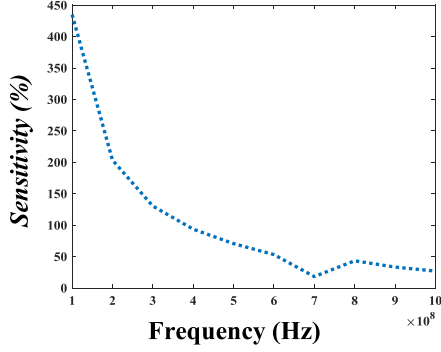


Fig. 3. Sensitivity of SE to Z_{ap} for a metallic enclosure with an aperture. The metallic enclosure dimensions are $300 \text{ mm} \times 300 \text{ mm} \times 12 \text{ mm}$. The aperture is located at the center of the front face and its dimensions are $100 \text{ mm} \times 5 \text{ mm}$. The monitor point is at the enclosure center ($p_x = 150 \text{ mm}$, $p_y = 150 \text{ mm}$, $p_z = 60 \text{ mm}$).

III. DE-EMBEDDING

In deriving the impedance Z using (7), the parasitic effects of SMA connectors and the MSL should be considered as the short, open, load, and thru (SOLT) calibration is performed only up to the SMA-connectors. Fig. 5(a) helps us to understand these parasitic effects. A model for the whole measurement setup is given in Fig. 5(b). The de-embedding procedure to remove the effects of the SMA-ports and MSLs on each side of the aperture is as follows.

In simulations using CST-MWS, the de-embedding process is easy to perform. From the post processing tab, one can calibrate the S -parameters to the edges of the aperture (see Fig. 6).

For experimental measurements, we propose the following process. As in Fig. 5, three networks are cascaded. The de-embedded S_{21} is equal to S_{21B} . The overall S_{21} for the three cascaded networks of Fig. 5(b) is [14]

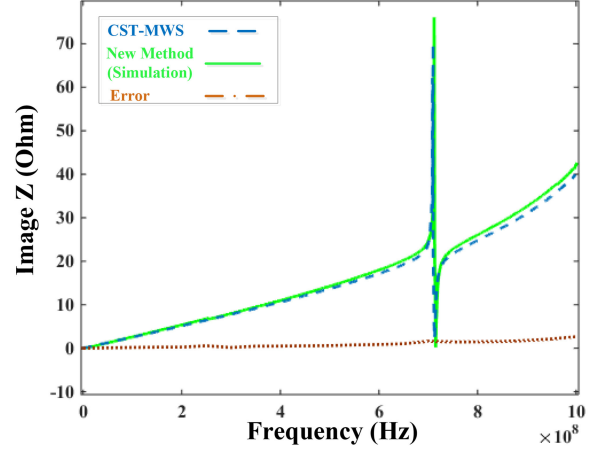
$$S_{21} = \frac{S_{21A} S_{21B} S_{21C}}{[1 - S_{22A} S_{11B} - S_{22B} S_{11C} + S_{22A} \Delta S_B S_{11C}]} \quad (11)$$

where $\Delta S_B = S_{11B} S_{22B} - S_{12B} S_{21B}$. Assuming S_{22A} and S_{11C} to be negligible (which is a fair assumption in case of an ideal 50Ω MSL), S_{21} can be estimated as

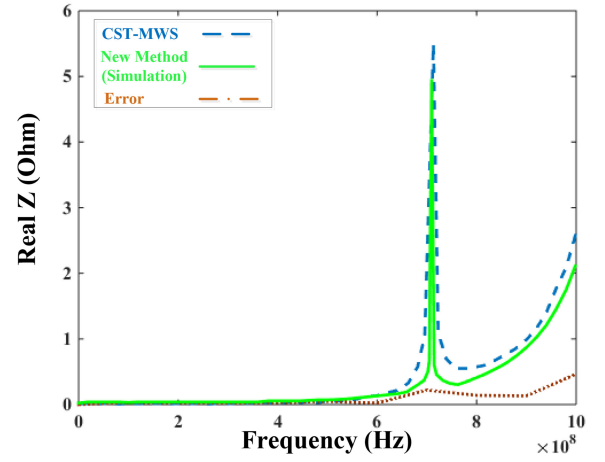
$$S_{21} = S_{21A} S_{21B} S_{21C}. \quad (12)$$

As S_{21B} is the parameter of interest, we need to perform another measurement on another face of the enclosure (a face with no aperture but with the same dimensions). The new cascaded networks for this setup are shown in Fig. 7. In this figure, A and C networks are equal to those of Fig. 5 (so they have the same S -parameters), but B' is an ideal MSL with the length of w . S_{21} of B' ($S_{21B'}$) is equal to

$$S_{21B'} = \frac{2}{A + B/Z_0 + CZ_0 + D}. \quad (13)$$



(a)



(b)

Fig. 4. Impedance between the two ports at point A (Z) for a metallic enclosure with a rectangular aperture. The metallic enclosure dimensions are $300 \text{ mm} \times 300 \text{ mm} \times 12 \text{ mm}$. The aperture is located at the center of the front face and its dimensions are $100 \text{ mm} \times 5 \text{ mm}$. (a) Imaginary part of Z . (b) Real part of Z .

In the above-mentioned equation, $ABCD$ parameters for a transmission line with length w can be calculated as [15]

$$A = \cos(\beta w) \quad (14)$$

$$B = jZ_0 \sin(\beta w) \quad (15)$$

$$C = \frac{j \sin(\beta w)}{Z_0} \quad (16)$$

$$D = \cos(\beta w) \quad (17)$$

$$\beta = 2\pi/\lambda. \quad (18)$$

As it can be seen, when w , compared to the wavelength, is small, we have $S_{21B'} \approx 1$. Now for the cascaded networks of Fig. 7

$$S'_{21} = S_{21A} S_{21B'} S_{21C}. \quad (19)$$

Since S'_{21} is measured using the setup of Fig. 7 and $S_{21B'}$ is estimated using (13), the product of S_{21A} and S_{21C} can be obtained and S_{21B} can be extracted precisely.

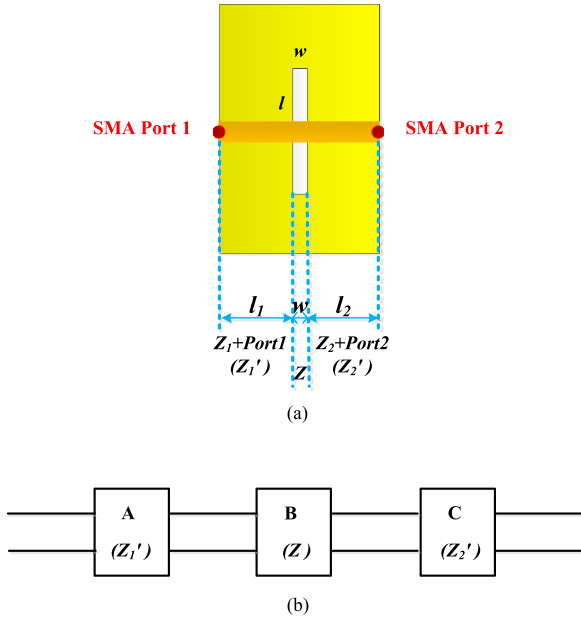


Fig. 5. (a) Top view of the measurement setup. (b) SMA port1 plus MSL with the length of l_1 , aperture impedance, and SMA port2 plus MSL with the length of l_2 are modeled as cascaded networks of A, B, and C, respectively.

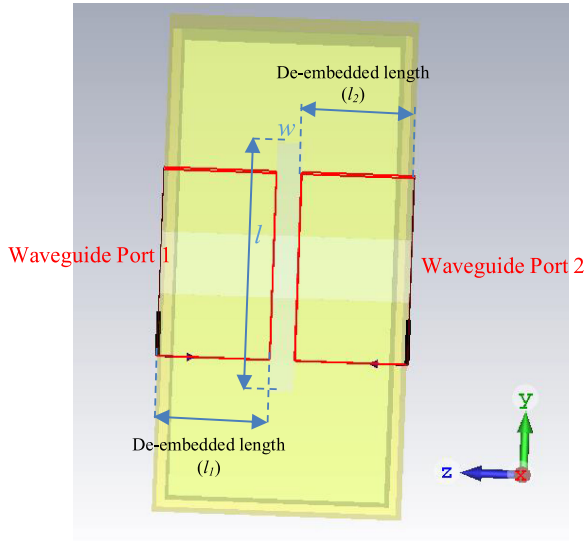


Fig. 6. Top view of the enclosure in CST-MWS medium. De-embedding is applied from the wave ports to the edge of the aperture.

IV. SIMULATION RESULTS

Fig. 8 shows the simulation results for the setup of Fig. 1. The width and height of the MSL are 3 mm and 0.6 mm, respectively. The resulted S_{21} is used to obtain the aperture impedance and finally, SE can be calculated using Robinson's formulation. The monitor point in this simulation is in the center of the enclosure. The enclosure dimensions are 40 mm \times 40 mm \times 20 mm and its thickness is 3 mm. The MSL length is 14 mm. The dimensions are set to form a 50 Ω MSL. These results are compared with the CST-MWS (frequency domain solver) simulation results.

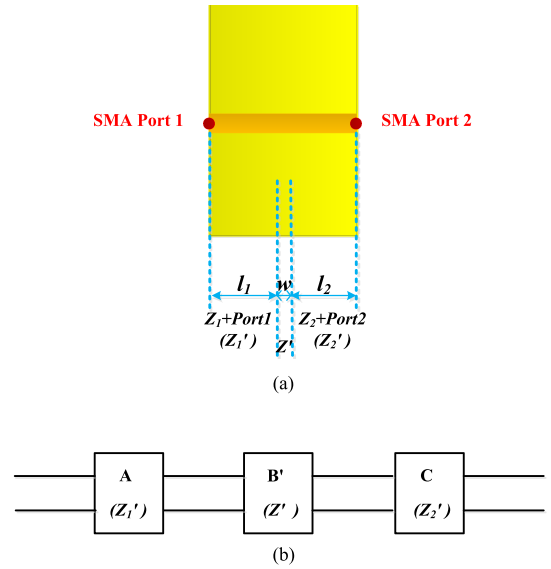


Fig. 7. (a) Top view of the enclosure with no aperture. (b) MSL with the length of aperture (previously existing aperture) and the SMA ports plus MSLs on either sides of the aperture are modeled as three cascaded networks (A, B', and C).

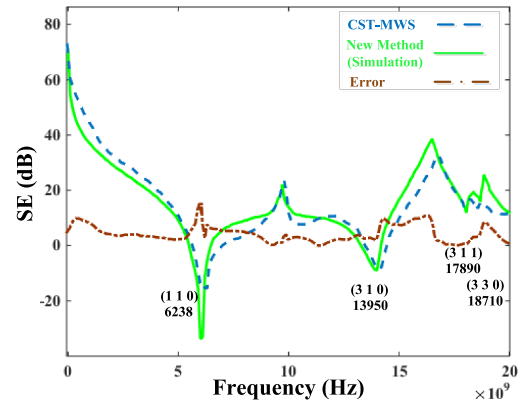


Fig. 8. Calculated SE for the test setup in Fig. 1. Our results are compared with CST-MWS results. The enclosure dimensions are 40 mm \times 40 mm \times 20 mm. The aperture is located at the center of the front face and its dimensions are 20 mm \times 2 mm. The width and height of the MSL are 3 mm and 0.6 mm, respectively. The monitor point is at the center of the enclosure ($p_x = 20$ mm, $p_y = 20$ mm, $p_z = 10$ mm). The resonance frequency of each mode is given in MHz.

The solver properties are as follows: frequency domain solver, tetrahedral (legacy) mesh type, accuracy of 10^{-9} , and mesh cells number of 352 725. A very good consistency between the results of the new method and CST-MWS, shows the applicability of the new method for extremely small dimension enclosures. For the off-center monitor point, the simulation results are shown in Fig. 9. As our approach considers losses in obtaining SE through the measured S -parameters, the resulted Z_{ap} has both real and imaginary parts.

In another case study, SE is simulated for an enclosure with a triangular aperture (see Fig. 10). The enclosure dimensions are 40 mm \times 40 mm \times 20 mm and its thickness is 3 mm.

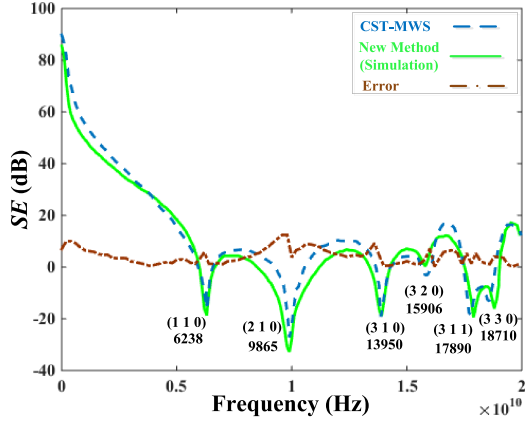


Fig. 9. Calculated SE for the test setup in Fig. 1. Our results are compared with CST-MWS results. The metallic enclosure dimensions are $40 \text{ mm} \times 40 \text{ mm} \times 20 \text{ mm}$. The aperture is located at the center of the front face and its dimensions are $20 \text{ mm} \times 2 \text{ mm}$. The monitor point is off-centered and it is located at $(p_x = 6 \text{ mm}, p_y = 20 \text{ mm}, p_z = 10 \text{ mm})$. The resonance frequency of each mode is given in MHz.

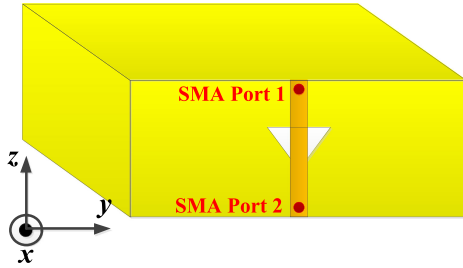


Fig. 10. Enclosure with a triangular aperture, the orange strip is the signal trace of a MSL where the enclosure is the ground plane of it.

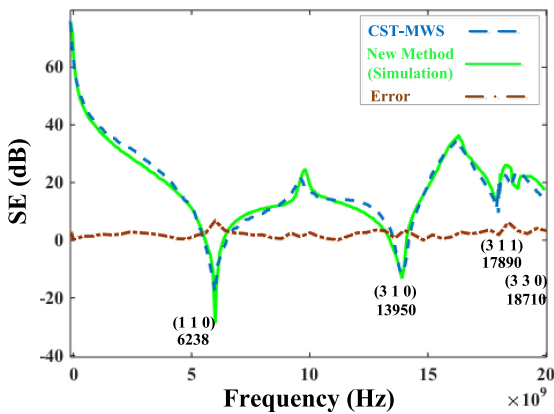


Fig. 11. Calculated SE for the test setup in Fig. 10. Our results are compared with corresponding CST-MWS results. The metallic enclosure dimensions are $40 \text{ mm} \times 40 \text{ mm} \times 20 \text{ mm}$. The aperture is an equilateral triangle with the side length of 6 mm , which is located at the center of the front face. The monitor point is at the center of the enclosure $(p_x = 20 \text{ mm}, p_y = 20 \text{ mm}, p_z = 10 \text{ mm})$. The resonance frequency of each mode is given in MHz.

The aperture is an equilateral triangle with each side length of 6 mm . The simulation results are compared with those of CST-MWS in Fig. 11. The consistency of these results also shows the capability of the new method for the enclosures with extremely small dimensions and arbitrary shape apertures.

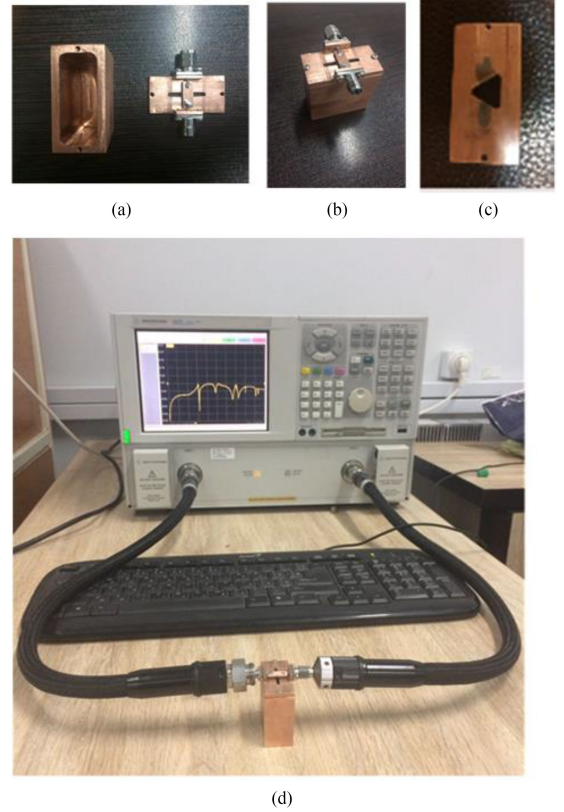


Fig. 12. Experimental test setup. (a) Empty enclosure beside its lid with the mounted MSL over the aperture. An SMA connector is connected with one side of each MSL. (b) Assembled DUT of enclosure with rectangular aperture. (c) Upper side of the enclosure with triangular aperture. The aperture side is 6 mm long. (d) Overall measurement setup. The measured S_{11} can be observed on the PNA monitor.

V. EXPERIMENTAL RESULTS

An experimental setup based on the new method is shown in Fig. 12. The enclosure that is the DUT is made of copper. Its dimensions are $40 \text{ mm} \times 40 \text{ mm} \times 20 \text{ mm}$ and its thickness is 3 mm . The aperture is located at the center of the front face and its dimensions are $20 \text{ mm} \times 2 \text{ mm}$. The MSL length is 14 mm . The experimental results are shown in Fig. 13 and compared with the simulation results and those of the CST-MWS. The experimental results tie well with the simulation and CST-MWS results. This confirms the reliability of the new method and its experimental setup for measuring SE of extremely small dimension enclosures. The sweep time for each measurement is approximately 3.3 s and each measurement is repeated 100 times. Therefore, a complete measurement requires 5.5 min . As we use the averaged value of 100 measurements, the noise effects and fluctuations are cancelled out. Furthermore, after SOLT calibration the maximum error in S -parameters is lower than -40 dB that has no considerable influence on the measured Z_{ap} .

The same experimental process is done with an enclosure with the same dimensions, but with a triangular aperture, see Fig. 12(c). The aperture is an equilateral triangle and its sides are 6 mm long. Its measured results are compared to the corresponding simulated results (our method and CST-MWS) in Fig. 14.

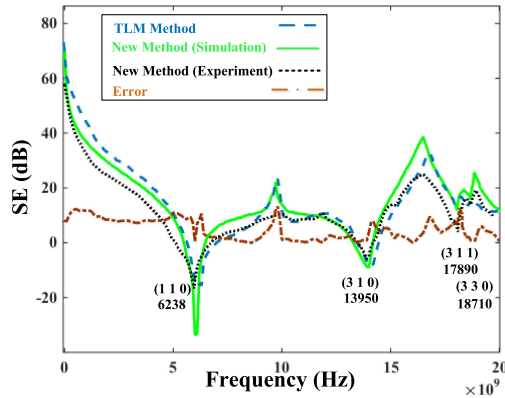


Fig. 13. SE for the test setup in Fig. 12(b). Our experimental results are compared with corresponding simulation results of the new method and CST-MWS results. The metallic enclosure dimensions are $40 \text{ mm} \times 40 \text{ mm} \times 20 \text{ mm}$. The aperture is located at the center of the front face and its dimensions are $20 \text{ mm} \times 2 \text{ mm}$. The monitor point is at the center of the enclosure ($p_x = 20 \text{ mm}$, $p_y = 20 \text{ mm}$, $p_z = 10 \text{ mm}$). The resonance frequency of each mode is given in MHz. The error curve shows the differences between the experimental and CST-MWS results.

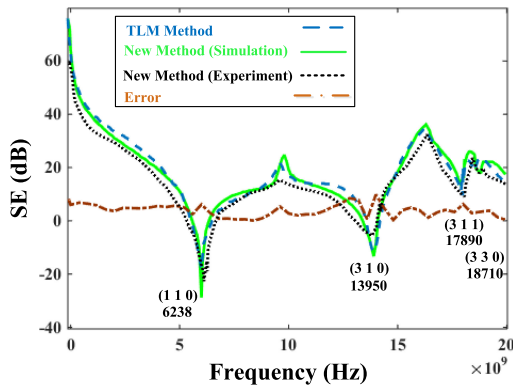


Fig. 14. SE for the enclosure in Fig. 12(c). Our experimental results are compared with corresponding simulation results of our method and CST-MWS results. The metallic enclosure dimensions are $40 \text{ mm} \times 40 \text{ mm} \times 20 \text{ mm}$. The aperture is triangular and it is located at the center of the front face. Each triangle side is 6 mm long. The monitor point is at the center of the enclosure ($p_x = 20 \text{ mm}$, $p_y = 20 \text{ mm}$, $p_z = 10 \text{ mm}$). The resonance frequency of each mode is given in MHz. The error curve shows the differences between the experimental and CST-MWS results.

VI. CONCLUSION

In this paper, a previously proposed method for SE estimation is applied to measure SE of extremely small dimension enclosures. The monitor point and the aperture shape are arbitrary in these simulations and measurements. The enclosure under test here has dimensions of $40 \text{ mm} \times 40 \text{ mm} \times 20 \text{ mm}$, which is far smaller than enclosures of previous reports.

The results are fairly consistent with simulated and experimental results. So, the new approach can be used as a reliable method for SE measurement of extremely small dimension enclosures. However, the method can only be applied if the field leakage is due to the aperture and the aperture is accessible so that an MSL can be attached to it.

Traditional methods for small shield enclosures require the use of a TEM cell, an anechoic, or reverberation chamber, along

with special probes inside the enclosure. Besides, while using these sensors and probes, we need precise designing of the measurement setup for each special DUT. But our proposed approach considering the practical hints explained in this paper can easily overcome these limitations and it can be implemented as a less time and the cost consuming method.

ACKNOWLEDGMENT

The authors would to acknowledge the support and help from all members of EMI/EMC and Microwave Technology Research Lab at Ferdowsi University of Mashhad, especially Dr. M. Forouzanfar for his support in doing the measurements.

REFERENCES

- [1] S. Celozzi, R. Araneo, and G. Lovat, *Electromagnetic shielding*. Hoboken, New Jersey: Wiley, 2008, pp. 42–46.
- [2] *IEEE Standard Method for Measuring the Shielding Effectiveness of Enclosures and Boxes Having All Dimensions Between 0.1 m and 2 m*, IEEE Standard 299.1-2013, 2014.
- [3] P. Young and L. Dawson, "Measurement of the shielding effectiveness of small enclosures using an optically coupled electric field sensor," in *Proc. 9th Int. Conf. Electromagn. Compat.*, Manchester, U.K., 1994, pp. 51–57.
- [4] Q. Wang, E. Cheng, and Z. Qu, "On the shielding effectiveness of small-dimension enclosures using a reverberation chamber," *IEEE Trans. Electromagn. Compat.*, vol. 53, no. 3, pp. 562–569, Aug. 2011.
- [5] R. Armstrong, A. C. Marvin, and J. F. Dawson, "Shielding effectiveness estimation of physically small electrically large enclosures through dimensional scaling," in *Proc. IEEE Int. Symp. Electromagn. Compat.*, Pittsburgh, PA, USA, 2012, pp. 652–656.
- [6] Z. Kubík and J. Skála, "Shielding effectiveness measurement and simulation of small perforated shielding enclosure using FEM," in *Proc. IEEE 15th Int. Conf. Environ. Elect. Eng.*, Rome, Italy, 2015, pp. 1983–1988.
- [7] A. Shourvarzi and M. Joodaki, "Shielding effectiveness estimation of a metallic enclosure with an aperture using S-parameter analysis: Analytic validation and experiment," *IEEE Trans. Electromagn. Compat.*, vol. 59, no. 2, pp. 537–540, Apr. 2017.
- [8] A. Shourvarzi and M. Joodaki, "Using aperture impedance for shielding effectiveness estimation of a metallic enclosure with multiple apertures on different walls considering higher order modes," *IEEE Trans. Electromagn. Compat.*, vol. 60, no. 3, pp. 629–637, Jun. 2017.
- [9] A. Shourvarzi and M. Joodaki, "Using a network of ports for shielding effectiveness optimization of an enclosure with arbitrary shape apertures," *Int. J. Numer. Model.*, 2018, Art. no. e2334. [Online]. Available: <https://doi.org/10.1002/jnm.2334>
- [10] A. Shourvarzi and M. Joodaki, "A fast method for estimating shielding effectiveness of an enclosure with apertures," in *Proc. Int. Symp. Electromagn. Compat. Eur.*, 2014, pp. 464–467.
- [11] A. Shourvarzi and M. Joodaki, "A network of ports to estimate shielding effectiveness of an enclosure with apertures," in *Proc. Int. Symp. Electromagn. Compat. Eur.*, 2016, pp. 626–630.
- [12] A. Shourvarzi and M. Joodaki, "Shielding effectiveness estimation of an enclosure with an arbitrary shape aperture," in *Proc. Int. Symp. Electromagn. Compat. Eur.*, 2017, pp. 1–4.
- [13] M. P. Robinson *et al.*, "Analytical formulation for the shielding effectiveness of enclosures with apertures," *IEEE Trans. Electromagn. Compat.*, vol. 40, no. 3, pp. 240–248, Aug. 1998.
- [14] R. Mavaddat, *Network Scattering Parameters* (Applied Mathematics). Singapore: World Scientific, 1996, pp. 50–51.
- [15] D. M. Pozar, *Microwave Engineering*, 4th ed. New York, NY, USA: Wiley, 2012.